Distributed Fixed-Time Control for Leader-Steered Rigid Shape Formation with Prescribed Performance

Distributed Fixed-Time Control for Leader-Steered Rigid Shape Formation with Prescribed Performance

Zhongchao Liang, *Member, IEEE*, Chunxiao Lyu, Mingyu Shen, *Student Member, IEEE*, Jing Zhao, Zhongguo Li, *Member, IEEE*, and Zhengtao Ding, *Senior Member, IEEE*

***Abstract*—Resorting to the principle of rigid body kinematics, a novel framework for a multi-robot network is proposed to form and maintain an invariant rigid geometric shape. Unlike consensus-based formation, this approach can perform both translational and rotational movements of the formation geometry, ensuring that the entire formation motion remains consistent with the leader. To achieve the target formation shape and motion, a distributed control protocol for multiple Euler-Lagrange robotic vehicles subject to nonholonomic constraints is developed. The proposed protocol includes a novel prescribed performance control (PPC) algorithm that addresses the second-order dynamics of the robotic vehicles by employing a combination of nonsingular sliding manifold and adaptive law. Finally, the effectiveness of the proposed formation framework and control protocol is demonstrated through the numerical simulations and practical experiments with a team of four robotic vehicles.**

***Index Terms*—Distributed control, fixed-time control, rigid shape geometry, prescribed performance constraint, multi-robot vehicles, nonholonomic constraint.**

I. Introduction

In the past few decades, the strategies for cooperation and coordination among multiple agents have attracted significant attention across various fields. Among these, the protocols of formation control have seen diverse advancements through distributed approaches [1]. These approaches have found wide applications in various agent types, such as unmanned surface vehicles (USVs) [2], connected automated vehicles (CAVs) [3], and wheeled mobile robots (WMRs) [4]-[5].

Practical applications often demand fast convergence in controlled systems [6]. In this context, the fixed-time control methodology presents a notable advantage by ensuring a bounded settling time, independent of initial conditions [7]. It outperforms finite-time and asymptotic control methods in terms of convergence performance, gaining substantial prominence in the domain of formation control strategies for multi-agent systems [8]-[10]. In the existing literature, both the homogeneous method and sliding mode control have been employed for designing fixed-time control laws [11]-[12]. However, the homogeneous method heavily relies on the homogeneity of system dynamics, facing challenges when unknown disturbances perturb the system. As a result, it often requires supplementary techniques, such as disturbance observers, to enhance its robustness [13]. In contrast, sliding mode control (SMC) stands out for its inherent capacity to fully compensate for matched uncertain dynamics and external disturbances, making it a more suitable choice for application in multi-robot systems facing uncertainties.

Beyond considering convergence rates and steady-state performance, transient performance throughout the entire control process plays a crucial role. Prescribed Performance Control (PPC) has been introduced to ensure that the state error remains within predefined bounds [14]. Subsequently, PPC protocols have been utilized in achieving formation control objectives across various multi-agent systems. For instance, in coordinating USVs, the PPC approach prevents collisions among formation members by mitigating potential excessive inputs in confined spaces [2]. In platoon formation control for CAVs, PPC-based controllers stabilize the entire queue and implement spacing strategies [3]. Within cooperative teams of WMRs, the PPC methodology confines robot states within sensor ranges [15]. Additionally, a PPC-based distributed formation cooperative algorithm has been proposed for a heterogeneous multi-agent system (MAS) comprising both Unmanned Aerial Vehicles (UAVs) and Unmanned Ground Vehicles (UGVs) to address potential actuator failures [16].

While PPC formation control approaches have successfully integrated fixed-time control techniques, these controlled systems are often described using single integrator models. However, in real-world applications, the kinematic control of single integrator models may not yield accurate results. In such scenarios, force or torque control methods designed for higher-order dynamics are essential for achieving superior performance. Consequently, cooperative control protocols have been extended to higher-order dynamics in multi-agent systems [17]-[18]. To tackle high-order systems, the backstepping algorithm and the adding a power integrator technique can be employed and integrated within fixed-time PPC protocols [19]-[21]. However, controllers based on the backstepping algorithm or the adding a power integrator often involve high-order derivatives of the virtual controller for the controlled high-order system, leading to the issue of derivative explosions.

This work was supported in part by the National Natural Science Foundation of China under Grants 51975109, in part by the Fundamental Research Funds for the Central Universities under Grant N2103018. (Corresponding author: Zhengtao Ding.)

Z. Liang, C. Lyu, M. Shen and J. Zhao are with the School of Mechanical Engineering and Automation, Northeastern University, Shenyang 110819, China. (e-mail: liangzc@me.neu.edu.cn; lyuchx@stumail.neu.edu.cn; shenmy@stumail.neu.edu.cn; zhaoj@mail.neu.edu.cn)

Z. Li and Z. Ding are with Department of Electrical and Electronic Engineering, University of Manchester, Manchester, M13 9PL, U.K. (email: zhongguo.li@manchester.ac.uk; zhengtao.ding@manchester.ac.uk).

In light of these considerations, this study aims to develop a nonsingular fixed-time sliding-mode approach for high-order systems to achieve formation control objectives while adhering to prescribed performance constraints.

Current research on distributed formation control with communication topologies predominantly revolves around control protocols that leverage the theoretical foundations of consensus control approaches [22]-[24]. In the consensus-based control approach, one of the control objectives is to achieve consensus in orientation among the agents [25]-[26]. Due to nonholonomic constraints, the instantaneous center of each robot lies on the line orthogonal to its velocity direction, corresponding to its orientation. Consequently, considering both the consensus objectives and the nonholonomic constraints, the lines orthogonal to the velocity direction of each robot become parallel when the robot group forms a rigid geometric relationship. As a result, the instantaneous center of the formed rigid geometry is located at an infinitely far-away position. This indicates that the consensus-based formation geometry is limited to performing only translational movement [22], [25], [27]-[29], lacking a shared center or rotational motion.

Despite the ability of consensus-based control protocols to achieve complex trajectories in formations [30]-[31], the absence of rotational motion in these formation geometries can lead to limitations in certain scenarios. To enrich manipulations of the rotational motion, we propose a novel framework called leader-steered rigid shape formation. This formation incorporates both translational and rotational movements, extending the capabilities of the leader to perform diverse tasks. In scenarios involving the transportation or docking of large-sized objects by multiple mobile robots, the formation geometry is typically designed to match the fixed shape of the objects. The inclusion of rotational movement in the formation allows for achieving the desired posture or orientation for successful docking, which cannot be accomplished by a consensus-based formation. Furthermore, in autonomous searching or exploration tasks, strategic positioning of certain robots at the front of the formation enables them to explore the unknown area and ensure the safety for their leader. In contrast, a consensus-based formation lacking rotational movement would result in the leading robot, initially positioned at the last spot, moving to the first position while the trajectory involves a turning of more than 180 degrees. Similarly, considering the sensing topology where the leader is placed at the first front to allow other agents' onboard cameras to capture crucial information, the absence of rotational movement in the formation geometry can lead to switches in the sensing topology as the formation order is altered. By highlighting these distinctions, it becomes evident that the inclusion of rotational movement in leader-steered rigid shape formations holds great importance for specific tasks, such as docking, exploration, and maintaining consistent sensing topologies. These tasks often require the formation to adapt its orientation or posture, which can only be achieved through the integration of rotational motion.

This paper addresses the challenge of integrating the distributed formation protocol with fixed-time control and prescribed performance control (PPC) schemes for multi-robot vehicle dynamics. Additionally, we explore the incorporation of directed graphs and the leader-steered rigid shape formation. Inspired by the preceding discussions, the primary innovations are highlighted as follows.

1) **Leader-Steered Rigid Shape Formation:** This study introduces a novel formation framework defined as "leader-steered rigid shape formation". The entire rigid geometric shape, connecting all agents, consistently follows the leader's movement. Notably, the proposed formation is capable of performing both translational and rotational movements based on the leader's motion.
2) **Sliding Mode and Prescribed Performance Control Algorithm:** We propose an innovative algorithm that combines sliding mode control and prescribed performance control to effectively address challenges posed by high-order systems, with a specific focus on achieving fixed-time convergence.
3) **Adaptive Algorithms with Prescribed Performance Control:** This study contributes theoretically to adaptive algorithms integrated with prescribed performance control when the system parameters and disturbance are completely unknown.

Compared with existing literature, our method exhibits novelty in several aspects:

1) In contrast to conventional consensus-based formation control [26]-[28], which primarily involves translational movements of the entire formation geometry, our innovative leader-steered rigid shape formation is guided by a leader performing both translational and rotational movements. Specifically designed for robots subject to nonholonomic constraints, resulting in bearing deviations among individual agents, our approach distinguishes from the extended consensus-based formation framework for holonomic robots [32].
2) Compared to existing leader-following formation models to achieve a rigid geometry [4], [33-34], our approach addresses limitations where all followers share a common leader.
3) The proposed control algorithm differs from traditional backstepping algorithms [20-21], [35], which may lead to derivative explosion due to calculations of multiple state derivatives. Our method incorporates a fixed-time nonsingular sliding manifold to mitigate this issue.
4) In contrast to existing research combining sliding mode control and prescribed performance control [36-38], typically assuming known system parameters and disturbance bounds, our work extends the applicability of this approach. We incorporate adaptive algorithms to address completely unknown system parameters and disturbances, achieving practical fixed-time convergence.

The subsequent sections are structured as follows: Section II encompasses the presentation of robotic dynamics, formation model, control objectives, and various lemmas. The design of the formation protocol is provided in Section III. Sections IV and V showcase the effectiveness of the proposed formation model and protocol through simulations and experiments. Finally, the conclusions are drawn in Section VI.

II. Problem Formulation

A. Dynamic model of robotic vehicles

Consider a formation system of multi-robot vehicles comprising of k followers and a leader denoted as L. The vehicles, indexed as i (i = L, 1, 2, ..., k), traverse the XOY plane, as illustrated in Fig. 1. Let m represent the vehicle mass, I_z represent the moment of inertia, $2l$ denote the distance between two driving wheels, and r denote the wheel radius. The position coordinates of the vehicle center p_{ci} for the ith vehicle can be expressed as $p_{ci} = [x_{ci}, y_{ci}]^{\mathrm{T}}$. The corresponding generalized coordinates are defined as $q_{ci} = [x_{ci}, y_{ci}, \theta_i]^{\mathrm{T}}$. The kinematic equation for vehicle i is defined as

$$\dot{q}_{ci} = E_i(\theta_i)\, v_i = \begin{bmatrix} \cos\theta_i & 0 \\ \sin\theta_i & 0 \\ 0 & 1 \end{bmatrix} \begin{bmatrix} v_{ci} \\ \omega_i \end{bmatrix} \tag{1}$$

where θ_i denotes the heading angle of i, while v_{ci} and ω_i represent the centroid velocity and angular velocity, respectively.

Subsequently, the Euler-Lagrange equation for q_{ci} in Cartesian coordinates can be formulated as

$$\begin{aligned} \bar{M}_i(q_{ci})\,\ddot{q}_{ci} + \bar{C}_i(\dot{q}_{ci}, q_{ci})\,\dot{q}_{ci} + \bar{Q}_i(q_{ci}) =& \bar{B}_i(q_{ci})\,\tau_i + \tau_{id} \\ &+ A_i^{\mathrm{T}}(q_{ci})\,\iota_i \end{aligned} \tag{2}$$

with

$$\bar{M}_i(q_{ci}) = \begin{bmatrix} m & 0 & 0 \\ 0 & m & 0 \\ 0 & 0 & I_z \end{bmatrix},\ \bar{C}_i(\dot{q}_{ci}, q_{ci}) = 0^{3\times 3}$$

$$\bar{B}_i(q_{ci}) = r^{-1} \begin{bmatrix} \cos\theta_i & \cos\theta_i \\ \sin\theta_i & \sin\theta_i \\ -l & l \end{bmatrix},$$

$$A_i(q_{ci}) = \begin{bmatrix} -\sin\theta_i & \cos\theta_i & 0 \end{bmatrix},$$

where $\bar{M}_i(q_{ci}) \in \mathbb{R}^{3\times 3}$ stands for the symmetric positive definite inertia matrix associated with the vehicle parameters; $\bar{C}_i(\dot{q}_{ci}, q_{ci}) \in \mathbb{R}^{3\times 3}$ is the Coriolis moment matrix; $\bar{Q}_i(q_{ci}) \in \mathbb{R}^{3\times 1}$ represents the unknown damping matrix; $\bar{B}_i(q_{ci}) \in \mathbb{R}^{3\times 2}$ denotes the input transformation matrix; $\tau_i = [\tau_{Li}, \tau_{Ri}]^{\mathrm{T}}$ designates the total torque of the left and right wheels, respectively, distributed among four wheels using the optimal principle [39]; $\tau_{id} \in \mathbb{R}^{2\times 1}$ incorporates the uncertainties, including the unknown $\bar{Q}_i(q_{ci})$; $A_i(q_{ci}) \in \mathbb{R}^{1\times 3}$ represents the nonholonomic constraint term with the constraint matrix $A_i(q_{ci})\dot{q}_{ci} = 0$; ι_i denotes the unknown Lagrange multiplier.

The dynamics description of vehicle i, with the nonholonomic constraint eliminated, is derived by substituting the time derivative of (1) into (2) and left-multiplying both sides by $E_i^{\mathrm{T}}(\theta_i)$, resulting in

$$M_i(q_{ci})\dot{v}_i + C_i(\dot{q}_{ci}, q_{ci})v_i = B_i(q_{ci})\tau_i + \tau_{id}, \tag{3}$$

with

$$M_i(q_{ci}) = E_i^{\mathrm{T}}\bar{M}_i E_i = \begin{bmatrix} m & 0 \\ 0 & I_z \end{bmatrix},$$

$$C_i(\dot{q}_{ci}, q_{ci}) = E_i^{\mathrm{T}}\left(\bar{M}_i E_i + \bar{C}_i E_i\right) = \mathbf{0}^{2\times 2},$$

$$B_i(\dot{q}_{ci}, q_{ci}) = E_i^{\mathrm{T}}\bar{B}_i = r^{-1}\begin{bmatrix} 1 & 1 \\ -l & l \end{bmatrix}.$$

The position of the vehicle head, denoted as $p_i = [x_i, y_i]^{\mathrm{T}}$, can be expressed as $p_i = [x_{ci} + hcos(\theta_i), y_{ci} + hsin(\theta_i)]^{\mathrm{T}}$, where h represents the offset from p_i to p_{ci}.

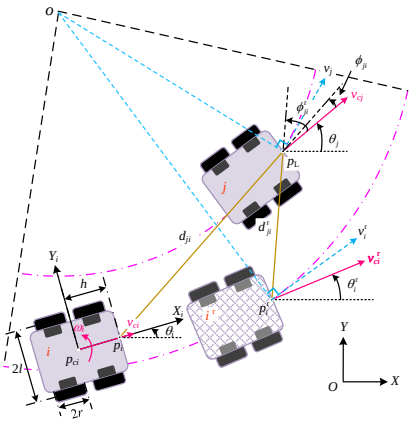

Fig. 1. Vehicle i and j are in (d, ϕ)-formation frame.

B. Graph Theory and Formation Tracking Error

Consider a group of $k+1$ robotic vehicles characterized by a directed graph $\mathcal{G} = \{\mathcal{O}, \mathcal{S}\}$, where $\mathcal{O}(\mathcal{G}) = \{\mathrm{L}, 1, 2, \cdots, k\}$ denotes the node set, and $\mathcal{S}(\mathcal{G}) = \{(j,i) : j \neq i,\ i, j \in \mathcal{O}(\mathcal{G})\}$ represents the collection of directed and connected edges. Specifically, $(j,i) \in \mathcal{S}(\mathcal{G})$ implies that vehicle j is a neighbor of vehicle i, allowing i to access information of j. Furthermore, the leading vehicle L serves as the starting point of the information flow and only acts as the neighbor of some other individuals in the network, *i.e.*, $\{(j, \mathrm{L}) : j \in \mathcal{O}(\mathcal{G})\} \nsubseteq \mathcal{S}(\mathcal{G})$ and $\{(\mathrm{L}, i) : i \in \mathcal{O}(\mathcal{G})\} \subseteq \mathcal{S}(\mathcal{G})$. It is assumed that the directed acyclic graph $\mathcal{G}$ contains a directed spanning tree, with the leading vehicle L serving as the root of the tree.

The adjacency matrix for graph $\mathcal{G}$ is denoted by $\mathcal{A}(\mathcal{G}) = \{a_{ij}\} \in \mathbb{R}^{(k+1)\times(k+1)}$ with $i, j \in \mathcal{O}(\mathcal{G})$, where $a_{ij} = 1$ with $i \neq j$ if $(i,j) \in \mathcal{S}(\mathcal{G})$, and $a_{ij} = 0$ otherwise. Notably, $a_{ii} = 0$ for $i \in \mathcal{O}(\mathcal{G})$. The directed Laplacian matrix for graph $\mathcal{G}$ is defined as $\mathcal{L}(\mathcal{G}) = \{l_{ij}\} \in \mathbb{R}^{(k+1)\times(k+1)}$, where $l_{ij} = \sum_{j=1}^{k} a_{ij}$ for $i = j$, and $l_{ij} = -a_{ij}$ for $i \neq j$.

To elucidate the formation control objective, the following definitions are introduced.

Definition 1: *Rigid shape formation.* A collection of $k+1$ robotic vehicles is considered to be in a *rigid shape formation*, if the Euclidean distance between any two agents remains constant. The constant desired distance d_{ji}^{r} between agents i and j is denoted as

$$d_{ji}^{\mathrm{r}} = \|p_i^{\mathrm{r}} - p_j\|^2 > 0,\ \forall j, i = \mathrm{L}, 1, 2, \cdots, k,$$

where $\|\cdot\|$ denotes the Euclidean norm; p_i^{r} represents the ideal position of p_i within the formation. It is noteworthy that the formation of a geometric shape within the team, involving $k+1$ vehicles, implies that $k \geq 2$.

Definition 2: *Leader-steered rigid shape formation.* Consider a directed acyclic graph comprising one leading robotic vehicle and k following robotic vehicles. This graph encompasses a directed spanning tree, where the leading robotic vehicle acts as the root of the tree. The robotic vehicle group is deemed to be in a *leader-steered rigid shape formation*, if it fulfills Definition 1, and the yaw motion of the entire

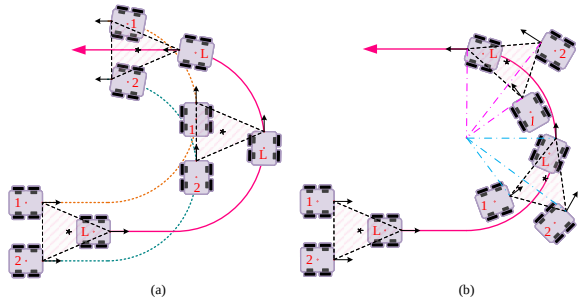

Fig. 2. Movement transformation of formation. (a) Formation translational, (b)Formation rotation.

geometric shape connecting all agents consistently aligns with the leading robotic vehicle.

In this paper, we propose a formation target aimed at creating and sustaining the ideal fixed geometry, as outlined in Definition 2, while taking into account the communication topology. The formation tracking error for the ith vehicle, following the local neighbor vehicle j, is defined as

$$e_{ji}(t) \triangleq p_i(t) - p_j(t) - D^{\mathrm{r}}_{ji}(t), \tag{4}$$

where $i \in \mathcal{O}(\mathcal{G})\backslash\{\mathrm{L}\}$, $j \in \mathcal{O}(\mathcal{G})$; $D^{\mathrm{r}}_{ji}(t) \in \mathbb{R}^{2\times 1}$ is the desired vector from vehicle j to vehicle i , and is defined as

$$D^{\mathrm{r}}_{ji}(t) = \begin{bmatrix} d^{\mathrm{r}}_{ji,x}(t) \\ d^{\mathrm{r}}_{ji,y}(t) \end{bmatrix} = \begin{bmatrix} -d^{\mathrm{r}}_{ji}\cos\left(\phi^{\mathrm{r}}_{ji}+\theta_j\right) \\ -d^{\mathrm{r}}_{ji}\sin\left(\phi^{\mathrm{r}}_{ji}+\theta_j\right) \end{bmatrix}, \tag{5}$$

where ϕ^{r}_{ji} denotes the angle between v_j and the vector from p_j to p^{r}_i; d^{r}_{ji} represents the desired relative distance between p^{r}_i and p_j, as illustrated in Fig.1.

Taking into account the communication topology, the formation tracking error regarding vehicle i is introduced as:

$$\eta_i(t) = p_i(t) + \sum_{j\in\mathcal{O}(\mathcal{G})\backslash\{i\}} \frac{l_{ij}}{l_{ii}}\left[p_j(t) + D^{\mathrm{r}}_{ji}(t)\right], \tag{6}$$

where $\eta_i(t) = [\eta_{i,x}(t), \eta_{i,y}(t)]^{\mathrm{T}} \in \mathbb{R}^{2\times 1}$, and $i \in \mathcal{O}(\mathcal{G})\backslash\{\mathrm{L}\}$.

Taking the second-order time derivative of (6) along (3) yields

$$\ddot{\eta}_i(t) = g_i(t) + J_i\tau_i + \delta_i(t), \tag{7}$$

where $\delta_i(t) \in \mathbb{R}^{2\times 1}$ involves the unmodel items and perturbations, and

$$J_i = \begin{bmatrix} J_{i,x} \\ J_{i,y} \end{bmatrix} = \begin{bmatrix} \frac{I_z\cos\theta_i + hlm\sin\theta_i}{I_z mr} & \frac{I_z\cos\theta_i - hlm\sin\theta_i}{I_z mr} \\ \frac{I_z\sin\theta_i - hlm\cos\theta_i}{I_z mr} & \frac{I_z\sin\theta_i + hlm\cos\theta_i}{I_z mr} \end{bmatrix},$$

$$g_i(t) = \begin{bmatrix} f_{i,x} + \sum\limits_{j\in\mathcal{O}\backslash\{i\}} \frac{l_{ij}}{l_{ii}}\left[f_{j,x} + d^{\mathrm{r}}_{ji}\omega_j^2\cos\left(\phi^{\mathrm{r}}_{ji}+\theta_j\right)\right] \\ f_{i,y} + \sum\limits_{j\in\mathcal{O}\backslash\{i\}} \frac{l_{ij}}{l_{ii}}\left[f_{j,y} - d^{\mathrm{r}}_{ji}\omega_j^2\sin\left(\phi^{\mathrm{r}}_{ji}+\theta_j\right)\right] \end{bmatrix},$$

$$\begin{bmatrix} f_{i,x} \\ f_{i,y} \end{bmatrix} = \begin{bmatrix} -v_{ci}\omega_i\sin\theta_i - \omega_i^2 h\cos\theta_i \\ v_{ci}\omega_i\cos\theta_i - \omega_i^2 h\sin\theta_i \end{bmatrix}.$$

By invoking the equivalent formation Lemma [39], the stabilization of the error dynamics (7) implies the stabilization for the formation tracking error defined in (4). Upon analyzing (6), it is evident that $\eta_{i,x}$ and $\eta_{i,y}$ appear in the same mathematical expressions with similar physical meanings. To simplify subsequent derivations, we employ $\eta_{i,a}$ with $a = x, y$ for brevity. With respect to $\delta_{i,a}$, we assume the existence of an unknown positive constant $\delta_{im,a}$ such that $|\delta_{i,a}| \le \delta_{im,a}$.

Remark 1: Definition 1 provides the entire formation geometry, while Definition 2 further specifies the motion of the entire formation geometry. Definition 1, when integrated with consensus bearing angles for multi-agent networks, has been proposed and achieved through consensus-based formation control protocols. Utilizing the kinematic law, the common instantaneous center of all agents is positioned infinite faraway, resulting in the entire geometry solely performing translational movements. In contrast, Definition 2 presents a framework where the translational and rotational movements of the invariant formation geometry are aligned with the leader's motion.

Remark 2: According to rigid graph theory, the stable and fixed geometry for the multi-robot network in Definition 1 must adhere to the requirement of the minimal rigid topology condition the minimal rigid topology condition when employing the distance formation model, known as the (d, d) pattern. To account for the local topology and the formation task for vehicle i, we introduce the (d, ϕ)-based formation model, incorporating the time-varying angle as given in (5). In comparison, consensus-based formation control can achieve the control target of $\lim\limits_{t\to\infty}|v_i - v_{\mathrm{L}}| = 0$ and $\lim\limits_{t\to\infty}|\omega_i - \omega_{\mathrm{L}}| = 0$, ensuring that the common instantaneous center of velocity of the formation members is consistently located at infinity, leading to translational motion only. This implies that within consensus-based formation, once the accumulated turning motion of the leader exceeds 180 degree, the leader loses its leading position, violating Definition 2, as depicted in Fig. 2(a). In contrast, the proposed time-varying parameter $D^{\mathrm{r}}_{ji}(t)$ enables the formation members to achieve the same velocity centroid, as shown in Fig. 1 and Fig. 2(b), and the leader remains at at the forefront of the team, satisfying Definition 2. Furthermore, the proposed formation model facilitates both translational and rotational motions of the formation, as illustrated in Fig. 2(b). In extended-consensus protocols, rotation movement has been discussed for fully-constrained agents in a formation system [32], such as a drone formation system and a Mecanum wheel robot system. However, for robotic vehicles subject to non-holonomic constraints, achieving the rotation of rigid formations, as depicted in Fig. 2(b), poses a challenge due to their inability to perform independent lateral movements of the vehicle body. Thus, the primary focus of this paper is to develop a leader-steered rigid shape formation algorithm for mobile robots subject to non-holonomic constraints.

Remark 3: It has been acknowledged that the fixed formation geometry cannot be achieved by the formation model based on the bearing angle offset of the following agent [5]. Therefore, the (d, ϕ) formation model in this paper is based on the bearing angle offset of the leading agent, and the actual time-varying velocity direction offsets among agents are considered in (5) to achieve fixed formation geometry. Notably, the following agents in the (d, ϕ) model of the existing research always share a common leader [2], [40]. Consequently, this paper also considers the topology among the multi-robotic vehicles, specifically addressing scenarios where the following agents do not share a common leader.

C. Formation Control Objective

To achieve the desired geometry and motion, $\eta_{i,a}$ plays a crucial role in determining the formation control performance. The following conditions are established for $\eta_{i,a}$.

1) Initial condition: At t = 0, the location of vehicle i satisfies the following constraint

$$\underline{\eta}_{i,a} < \eta_{i,a}(0) < \bar{\eta}_{i,a}, \quad i = 1, \cdots, k, \tag{8}$$

where $\underline{\eta}_{i,a} \in \mathbb{R}$ and $\bar{\eta}_{i,a} \in \mathbb{R}$ represent the minimum and maximum ranges of $\eta_{i,a}(0)$, ensuring $\underline{\eta}_{i,a} < 0$ and $\bar{\eta}_{i,a} > 0$, respectively.

2) Prescribed performance boundary: If (8) holds, the formation target is predefined to satisfy the following constraint

$$\eta_{i,a}(t) \in \Omega_{i,a}, \quad \forall t \geq 0, \tag{9}$$

where $\Omega_{i,a} = \{\eta_{i,a}(t) | - k_{i\eta,a}\rho_{i,a}(t) \leq \eta_{i,a}(t) \leq \rho_{i,a}(t)\}$, $k_{i\eta,a}$ is a positive gain, and the decay boundary function $\rho_{i,a}(t)$ is defined as

$$\rho_{i,a}(t) = (\rho_{i0,a} - \rho_{i\infty,a}) e^{-k_{i\rho,a}t} + \rho_{i\infty,a}, \tag{10}$$

in which, $k_{i\rho,a}$ is a positive design parameter, $\rho_{i0,a} = \bar{\eta}_{i,a}$, and $\rho_{i\infty,a}$ represents the steady-state boundary of $\eta_{i,a}$ with $0 < \rho_{i\infty,a} < \rho_{i0,a}$. Deriving from (8) and (9), it is evident that $k_{i\eta,a} = -\underline{\eta}_{i,a}/\bar{\eta}_{i,a} > 0$.

With these considerations, we can specify the distributed formation control objectives as follows.

1) Fixed-time Convergence: The formation tracking errors $\eta_{i,a}$ exhibit fixed-time convergence to the residual set of (9), forming a neighborhood of zero.

2) Prescribed Performance: Throughout the entire formation tracking process, the formation tracking errors $\eta_{i,a}$ consistently adhere to the prescribed performance constraints (9).

Furthermore, achieving the above control objectives ensures the formation and maintenance of the leader-steered rigid shape formation as defined in Definition 2.

D. Preliminaries

Lemma 1: [10] For $x_i \geq 0$, $i = 1, \cdots, n$, it follows

$$\sum_{i=1}^{n} x_i^p \geq \left(\sum_{i=1}^{n} x_i\right)^p, \qquad 0 < p \leq 1;$$
$$\sum_{i=1}^{n} x_i^p \geq n^{1-p}\left(\sum_{i=1}^{n} x_i\right)^p, \qquad p > 1.$$

Lemma 2: For $\dot{x} = f(x)$, consider a continuous positive definite and radially unbounded function $V(x)$. Suppose the following inequality holds

$$\dot{V} \leq -\alpha V^p - \beta V^q + \gamma V^m + \varphi V^n + C,$$

where $\alpha, \beta, \gamma, \varphi, C, p, q, m, n$ are all positive constants satisfying $p > m > n > 1 > q$ and $C < \infty$. Then, the system can globally converge to the following set

$$V(x) \leq V_{\mathrm{M}} = \max\left\{ \sqrt[p-m]{\frac{\gamma}{\varpi_1\alpha}}, \sqrt[p-n]{\frac{\varphi}{\varpi_2\alpha}}, \sqrt[p]{\frac{C}{\varpi_3\alpha}} \right\}, \tag{11}$$

in a fixed-time, and the positive scalars $\varpi_1, \varpi_2, \varpi_3$ satisfy $\varpi_1 + \varpi_2 + \varpi_3 \in (0, 1)$. Furthermore, the fixed settling time T is constrained by

$$T \leq T_{\max} = \frac{1}{\left(1 - \sum_{c=1}^{3} \varpi_c\right)\alpha(p-1)} + \frac{1}{\beta(1-q)}. \tag{12}$$

Proof: If a system $\dot{x} = f(x)$ satisfies the fixed-time theory as discussed in [41], then, for $\sum_{c=1}^{3} \varpi_c \in (0, 1)$, the following inequality holds

$$\begin{aligned}\dot{V} \leq & -(1 - \varpi_1 - \varpi_2 - \varpi_3)\alpha V^p - \beta V^q + (\gamma V^m - \varpi_1\alpha V^p) \\ & + (\varphi V^n - \varpi_2\alpha V^p) + (C - \varpi_3\alpha V^p).\end{aligned} \tag{13}$$

If $V(x)$ fails to satisfy (11), then the following inequality holds

$$\begin{cases} \gamma V^m - \varpi_1\alpha V^p < 0 \\ \varphi V^n - \varpi_2\alpha V^p < 0 \\ C - \varpi_3\alpha V^p < 0 \end{cases}. \tag{14}$$

In accordance with the fixed-time theory [41], x will converge to the set defined by (11) within a fixed time under the influence of the negative $\dot{V}$. The convergence time can be estimated using (12). This concludes the proof. ■

Lemma 3: If $\forall z \in \mathbb{R}$, then it holds that $0 \leq z[\mathrm{sign}(z) - \mathrm{sat}(z)] \leq k_{\mathrm{sat}}^{-1}$, with

$$\mathrm{sat}(z) = \begin{cases} k_{\mathrm{sat}} z, & -k_{\mathrm{sat}}^{-1} < z < k_{\mathrm{sat}}^{-1} \\ \mathrm{sign}(z), & \text{else} \end{cases}.$$

III. Controller Design

A. Fixed-time Convergence of Sliding Manifold

In order to achieve the fixed-time convergence rate, we employ the following nonsingular sliding mode manifold [12]

$$S_{i,a} = \eta_{i,a} + [\psi(\eta_{i,a})\dot{\eta}_{i,a}]^{q_s/p_s}, \tag{15}$$

with

$$\psi(\eta_{i,a}) = \left(\alpha_{i,a}\eta_{i,a}^{m_s/n_s - p_s/q_s} + \beta_{i,a}\right)^{-1},$$

where $\alpha_{i,a}$ and $\beta_{i,a}$ are positive constants; m_s, n_s, p_s and q_s are positive odd integers, satisfying $2p_s > q_s > p_s, m_s > n_s$ and $m_s/n_s - p_s/q_s > 1$. For simplicity, $\psi(\eta_{i,a})$ is abbreviated as $\psi_{i,a}$ in subsequent contexts.

To satisfy (8), the initial condition for $S_{i,a}$ is defined as

$$\underline{S}_{i,a} \leq S_{i,a}(0) \leq \bar{S}_{i,a}, \tag{16}$$

where $\underline{S}_{i,a}$ and $\bar{S}_{i,a}$ represent the minimum and maximum ranges of the initial state of $S_{i,a}$, respectively.

Then, the following set is predefined for the sliding manifold

$$S_{i,a}(t) \in \Omega_{si,a}^{\mathrm{r}}, \quad \forall t \geq 0, \tag{17}$$

where $\Omega_{si,a}^{\mathrm{r}} = \{S_{i,a}(t) | - k_{is,a}k_{i\eta,a}\rho_{i,a}(t) \leq S_{i,a}(t) \leq k_{is,a}\rho_{i,a}(t)\}$, and $k_{is,a}$ is a positive gain satisfying $0 < k_{is,a} < 1$. In the next section, we will provide the proof that the PPC objective can be achieved if the preset constraint set (17) can be guaranteed.

To address the singularity issue associated with the sliding manifold (15), the following function is employed:

$$\mu(\dot{\eta}_{i,a}^{q_s/p_s-1}) = \begin{cases} 1, & |\dot{\eta}_{i,a}| > \sigma^{p_s/(q_s-p_s)} \\ \dot{\eta}_{i,a}^{q_s/p_s-1}/\sigma, & |\dot{\eta}_{i,a}| \le \sigma^{p_s/(q_s-p_s)} \end{cases}, \quad (18)$$

where $\sigma > 0$. For simplicity, $\mu\left(\dot{\eta}_{i,a}^{q_s/p_s-1}\right)$ is abbreviated as $\mu_{i\eta,a}$ in subsequent contexts.

Define $\xi_{i,a}(t) = S_{i,a}(t)\rho_{i,a}^{-1}(t)k_{is,a}^{-1}$, and transform the predefined set (17) to $\xi_{i,a}(t) \in (-k_{i\eta,a}, 1)$. Then, the following theorem outlines the first sliding-mode convergent process.

Theorem 1: For the error dynamics in (7), given the initial condition (16), suppose a virtual control input $u_i = [u_{i,x}, u_{i,y}]^{\mathrm{T}} = J_i\tau_i$. Consider the following distributed formation controller

$$u_{i,a} = -\psi_{i,a}^{-1}\left(u_{i1,a} + u_{i2,a} + u_{i3,a}\right), \quad (19)$$

with

$$\begin{cases} u_{i1,a} = \psi_{i,a}(g_{i,a} + \hat{\delta}_{im,a}\mathrm{sat}(\zeta_{i2,a})), \\ u_{i2,a} = \left[\frac{q_s}{p_s}(\psi_{i,a}\dot{\eta}_{i,a})^{q_s/p_s-1}\right]^{-1}\Big[\dot{\eta}_{i,a} - \mu_{i\eta,a}k_{is,a}\xi_{i,a} \\ \qquad \times\left(\dot{\rho}_{i,a} - \frac{k_{i\xi,a}k_{i\eta,a}^2\rho_{i,a}}{(1-\xi_{i,a})(\xi_{i,a}+k_{i\eta,a})}\right)\Big], \\ u_{i3,a} = -\alpha_{i,a}\left(m_s/n_s - p_s/q_s\right)\eta_{i,a}^{m_s/n_s-p_s/q_s-1}(\psi_{i,a}\dot{\eta}_{i,a})^2, \end{cases}$$

updated by

$$\dot{\hat{\delta}}_{\mathrm{im},a} = \kappa_{i1,a}\zeta_{i2,a}\left(\xi_{i,a}, \eta_{i,a}, \dot{\eta}_{i,a}\right)\mathrm{sat}\left(\zeta_{i2,a}\right) - \kappa_{i2,a}\hat{\delta}_{\mathrm{im},a}^3, \quad (20)$$

with positive control gains $k_{i\xi,a}$, $\kappa_{i1,a}$, $\kappa_{i2,a}$, and $\zeta_{i2,a}$ given below (24). Then, $S_{i,a}$ will converge to the following small residual set of (17) while $t \ge T_{is,a}$,

$$\Omega_{si,a} = \left\{S_{i,a}\left(t\right)|\underline{\xi}_{is,a}k_{is,a}\rho_{i,a}\left(t\right) \le S_{i,a} \le \bar{\xi}_{is,a}k_{is,a}\rho_{i,a}\left(t\right)\right\}, \quad (21)$$

where $\underline{\xi}_{is,a}$ and $\bar{\xi}_{is,a}$ are provided in (30); $T_{is,a}$ represents the estimated time for the sliding surface $S_{i,a}$ to converge to the specified region (21), and is given in (31). Meanwhile, the predefined performance boundaries for $S_{i,a}(t)$ in (17) will be guaranteed. Additionally, the actual wheel torque input can be calculated as $\tau_i = J_i^{-1}u_i$.

Remark 4: In the proposed controller in (19), it is evident that, when $\dot{\eta}_{i,a} = 0$ and (18) is not employed, a singularity issue arises in $u_{i2,a}$. Conversely, with the utilization of (18), if $\left|\dot{\eta}_{i,a}\right| > \sigma^{p_s/(q_s-p_s)}$, we have $\mu_{i\eta,a} = 1$, indicating that (18) remains inactivated, and the singularity will not occur. However, when $\left|\dot{\eta}_{i,a}\right| \le \sigma^{p_s/(q_s-p_s)}$, and we substitute (18) into $u_{i2,a}$, the singularity issue can be effectively resolved.

Remark 5: According to the definitions of sets $\Omega_{i,a}^r$ and $\Omega_{si,a}^r$ in (9) and (17), respectively, we observe that the parameters $k_{i\eta,a}$ and $k_{is,a}$, along with $\rho_{i0,a}$ within $\rho_{i,a}\left(t\right)$, are positive designable parameters directly related to the initial conditions. Since we have complete knowledge of the initial states within the formation system, $k_{i\eta,a}$, $k_{is,a}$ and $\rho_{i0,a}$ offer us the flexibility to make appropriate selections. This adaptability allows us to define the prescribed performance boundary, ensuring the inclusion of the initial conditions for both $\eta_{i,a}$ and $S_{i,a}$. Consequently, this arrangement guarantees that $\eta_{i,a}\left(0\right)$ resides within set $\Omega_{i,a}^r$, and $S_{i,a}\left(0\right)$ is situated within the set $\Omega_{si,a}^r$.

Proof: Firstly, introduce the homeomorphism mapping from $\xi_{is,a}(t)$ to $z_{i,a}(t)$ as follows

$$z_{i,a} = k_{i\eta,a}\xi_{i,a}[(1-\xi_{i,a})(\xi_{i,a}+k_{i\eta,a})]^{-1}. \quad (22)$$

The time derivative of $z_{i,a}$ is $\dot{z}_{i,a} = \frac{\left(k_{i\eta,a}+{\xi_{i,a}}^2\right)\dot{\xi}_{i,a}k_{i\eta,a}}{[(1-\xi_{i,a})(\xi_{i,a}+k_{i\eta,a})]^2}$.

Select the Lyapunov function candidate as

$$V_{iz,a} = z_{i,a}^2/2 + \kappa_{i1,a}^{-1}\tilde{\delta}_{\mathrm{im},a}^2/2, \quad (23)$$

where $\kappa_{i1,a}$ is a positive control gain, and $\tilde{\delta}_{\mathrm{im},a} = \hat{\delta}_{\mathrm{im},a} - \delta_{\mathrm{im},a}$.

Differentiating (23) and applying the proposed controller (19) produce

$$\begin{aligned} \dot{V}_{iz,a} = & -\mu_{i\eta,a}\frac{k_{i\xi,a}k_{i\eta,a}^4\xi_{i,a}^2\left(k_{i\eta,a}+\xi_{i,a}^2\right)}{[(1-\xi_{i,a})(\xi_{i,a}+k_{i\eta,a})]^4} \\ & -\left[1-\mu_{i\eta,a}\right]\zeta_{i1,a}k_{is,a}\xi_{i,a}\dot{\rho}_{i,a} \\ & +\zeta_{i2,a}\left[\delta_{i,a} - \hat{\delta}_{\mathrm{im},a}\mathrm{sat}\left(\zeta_{i2,a}\right)\right] + \kappa_{i1,a}^{-1}\dot{\hat{\delta}}_{\mathrm{im},a}\tilde{\delta}_{\mathrm{im},a} \\ \le & -\mu_{i\eta,a}k_{i\xi,a}z_{i,a}^4 - \left[1-\mu_{i\eta,a}\right]\zeta_{i1,a}k_{is,a}\xi_{i,a}\dot{\rho}_{i,a} \\ & +\zeta_{i2,a}\left[\delta_{i,a} - \hat{\delta}_{\mathrm{im},a}\mathrm{sat}\left(\zeta_{i2,a}\right)\right] + \kappa_{i1,a}^{-1}\dot{\hat{\delta}}_{\mathrm{im},a}\tilde{\delta}_{\mathrm{im},a}, \end{aligned} \quad (24)$$

where

$$\begin{aligned} \zeta_{i1,a} &= \frac{k_{i\eta,a}^2\xi_{i,a}\left(k_{i\eta,a}+\xi_{i,a}^2\right)}{[(1-\xi_{i,a})(\xi_{i,a}+k_{i\eta,a})]^3k_{is,a}\rho_{i,a}} \\ \zeta_{i2,a} &= \frac{q_s}{p_s}(\psi_{i,a}\dot{\eta}_{i,a})^{q_s/p_s-1}\frac{\psi_{i,a}k_{i\eta,a}^2\xi_{i,a}\left(k_{i\eta,a}+\xi_{i,a}^2\right)}{[(1-\xi_{i,a})(\xi_{i,a}+k_{i\eta,a})]^3k_{is,a}\rho_{i,a}} \end{aligned}.$$

From (10), we can obtain

$$0 \le \frac{-\dot{\rho}_{i,a}}{\rho_{i,a}} = k_{i\rho,a}\left[1 + \frac{\rho_{i\infty,a}}{\left(\rho_{i0,a}-\rho_{i\infty,a}\right)e^{-k_{i\rho,a}t}}\right]^{-1} \le k_{i\rho,a}. \quad (25)$$

In addition, the following inequality can be obtained

$$\begin{aligned} -\zeta_{i1,a}k_{is,a}\xi_{i,a}\dot{\rho}_{i,a} &= \frac{-\dot{\rho}_{i,a}}{\rho_{i,a}}z_{i,a}^2\left[\frac{(2\xi_{i,a}+k_{i\eta,a}-1)\xi_{i,a}}{(1-\xi_{i,a})(\xi_{i,a}+k_{i\eta,a})}+1\right] \\ &\le \frac{k_{i\rho,a}}{k_{i\eta,a}}h_{i,a}|z_{i,a}|^3 + k_{i\rho,a}z_{i,a}^2, \end{aligned} \quad (26)$$

where $h_{i,a} = 2\max(1, k_{i\eta,a}) + |1-k_{i\eta,a}|$.

Invoking Lemma 1 and Lemma 3, and substituting (20), (25) and (26) into (24) produce

$$\begin{aligned} \dot{V}_{iz,a} \le & \left[1-\mu_{i\eta,a}\right]\left(\frac{k_{i\rho,a}}{k_{i\eta,a}}h_{i,a}|z_{i,a}|^3 + k_{i\rho,a}z_{i,a}^2\right) \\ & -\mu_{i\eta,a}k_{i\xi,a}z_{i,a}^4 - \kappa_{i1,a}^{-1}\kappa_{i2,a}\hat{\delta}_{\mathrm{im},a}^3\tilde{\delta}_{\mathrm{im},a} + \delta_{\mathrm{im},a}k_{\mathrm{sat}}^{-1} \\ \le & \left[1-\mu_{i\eta,a}\right]\left(\frac{k_{i\rho,a}}{k_{i\eta,a}}h_{i,a}|z_{i,a}|^3 + k_{i\rho,a}z_{i,a}^2\right)\mu_{i\eta,a} \\ & -\mu_{i\eta,a}k_{i\xi,a}z_{i,a}^4 - \kappa_{i1,a}^{-1}\kappa_{i2,a}b_{i1,a}\tilde{\delta}_{\mathrm{im},a}^4 \\ & +\kappa_{i1,a}^{-1}\kappa_{i2,a}b_{i2,a}\delta_{\mathrm{im},a}^4 + \delta_{\mathrm{im},a}k_{\mathrm{sat}}^{-1} \\ \le & \left[1-\mu_{i\eta,a}\right]\left(\frac{k_{i\rho,a}}{k_{i\eta,a}}h_{i,a}|z_{i,a}|^3 + k_{i\rho,a}z_{i,a}^2\right) \\ & -\frac{1}{2}\left[\mu_{i\eta,a}k_{i\xi,a}z_{i,a}^4 + \kappa_{i1,a}^{-1}\kappa_{i2,a}b_{i1,a}\tilde{\delta}_{\mathrm{im},a}^4\right] \\ & -\frac{1}{4}\left[\mu_{i\eta,a}k_{i\xi,a}z_{i,a}^{2\lambda_{i,a}} + \kappa_{i1,a}^{-1}\kappa_{i2,a}b_{i1,a}\tilde{\delta}_{\mathrm{im},a}^{2\lambda_{i,a}}\right] + C_{i,a} \\ \le & -\chi_{i1,a}V_{iz,a}^2 - \chi_{i2,a}V_{iz,a}^{\lambda_{i,a}} + \left[1-\mu_{i\eta,a}\right]\frac{k_{i\rho,a}}{k_{i\eta,a}}h_{i,a}V_{iz,a}^{3/2} \\ & +\left[1-\mu_{i\eta,a}\right]k_{i\rho,a}V_{iz,a} + C_{i,a}, \end{aligned} \quad (27)$$

where $0 < \lambda_{i,a} < 1$; $b_{i1,a}$ and $b_{i2,a}$ are positive constants satisfying $-\varsigma_1(\varsigma_1+\varsigma_2)^3 \le -b_{i1,a}\varsigma_1^4 + b_{i2,a}\varsigma_2^4$ with $b_{i1,a} =$

$1-9/4\varpi$ and $b_{i2,a}=3/4\varpi^3-1/12$, where $\varpi>0,\varsigma_1,\varsigma_2\in\mathbb{R}$. The other parameters in (27) can be calculated by

$$\begin{aligned}\chi_{i1,a}&=2^{-1}\min\left\{\mu_{i\eta,a}k_{i\xi,a},\kappa_{i1,a}^{-1}\kappa_{i2,a}b_{i1,a}\right\},\\ \chi_{i2,a}&=2^{\lambda_{i,a}-2}\min\left\{\mu_{i\eta,a}k_{i\xi,a},\kappa_{i1,a}^{-1}\kappa_{i2,a}b_{i1,a}\right\},\\ C_{i,a}&=\kappa_{i1,a}^{-1}\kappa_{i2,a}b_{i2,a}\delta_{\mathrm{im},a}^4+2^{-1}\left(k_{i\xi,a}+\kappa_{i2,a}b_{i1,a}\right)\\&\quad+\delta_{\mathrm{im},a}k_{\mathrm{sat}}^{-1}.\end{aligned}\tag{28}$$

While $|\dot{\eta}_{i,a}|>\sigma^{p_s/(q_s-p_s)}$, resorting to Lemma 2, $z_{i,a}$ can be driven to the following limited region in a fixed time

$$\left|\frac{k_{i\eta,a}\xi_{i,a}}{\left(1-\xi_{i,a}\right)\left(\xi_{i,a}+k_{i\eta,a}\right)}\right|=|z_{i,a}|\leq z_{i\mathrm{m},a}\leq\sqrt{2V_{iz\mathrm{m},a}},\tag{29}$$

with

$$V_{iz\mathrm{m},a}=\max\left\{\left(\frac{1-\mu_{i\eta,a}}{\varpi_{i3,a}\chi_{i1,a}}\right)^2,\frac{1-\mu_{i\eta,a}}{\varpi_{i2,a}\chi_{i1,a}},\left(\frac{C}{\varpi_{i1,a}\chi_{i1,a}}\right)^{\frac{1}{2}}\right\},$$

where $\varpi_{i1,a},\varpi_{i2,a}$ and $\varpi_{i3,a}$ are positive parameters satisfying $\varpi_{i1,a}+\varpi_{i2,a}+\varpi_{i3,a}\in(0,1)$.

While $\mu_{i\eta,a}=1$ with $|\dot{\eta}_{i,a}|>\sigma^{p_s/(q_s-p_s)}$, $z_{i,a}$ will converge to a small compact set bounded by $z_{i\mathrm{m},a}\leq\sqrt{2}[C_{i,a}/(\varpi_{i1,a}\chi_{i1,a})]^{1/4}$ in a fixed time. While $\mu_{i\eta,a}\in(0,1)$ with $\dot{\eta}_{i,a}\neq0$, the fixed-time convergent rate of $\eta_{i,a}$ can still be guaranteed by $\mu_{i\eta,a}\neq0$. If $\dot{\eta}_{i,a}=0$ and $\eta_{i,a}\neq0$, $\ddot{\eta}_{i,a}\neq0$ can be calculated by substituting the torque input τ_i given by Theorem 1 into the error dynamics in (7). This implies that $\dot{\eta}_{i,a}$ will not remain at zero, and will transgress $|\dot{\eta}_{i,a}|<\sigma^{p_s/(q_s-p_s)}$ into $|\dot{\eta}_{i,a}|\geq\sigma^{p_s/(q_s-p_s)}$ within a finite time $t_{ir,a}$, which can be made very small through selecting a sufficiently small σ [12]. The detailed analysis can be found in the Appendix.

From (29), we can solve the residual set for $\xi_{i,a}$ as

$$\underline{\xi}_{is,a}\leq\xi_{i,a}\left(t\right)\leq\bar{\xi}_{is,a},\quad t>T_{is,a}\tag{30}$$

where

$$\begin{cases}\underline{\xi}_{is,a}=\frac{1}{2}\left[\left(1-k_{i\eta,a}+k_{i\eta,a}z_{i\mathrm{m},a}^{-1}\right)\right.\\\qquad\left.-\sqrt{\left(1-k_{i\eta,a}+k_{i\eta,a}z_{i\mathrm{m},a}^{-1}\right)^2+4k_{i\eta,a}}\right]\\ \bar{\xi}_{is,a}=\frac{1}{2}\left[\left(1-k_{i\eta,a}-k_{i\eta,a}z_{i\mathrm{m},a}^{-1}\right)\right.\\\qquad\left.+\sqrt{\left(1-k_{i\eta,a}-k_{i\eta,a}z_{i\mathrm{m},a}^{-1}\right)^2+4k_{i\eta,a}}\right]\end{cases}.$$

Invoking Lemma 2, the settling time can be estimated by

$$\begin{aligned}T_{is,a}=&\left[\chi_{i1,a}\left(1-\sum_{c=1}^{3}\varpi_{ic,a}\right)\right]^{-1}\\&+\left[\chi_{i2,a}\left(1-\lambda_{i,a}\right)\right]^{-1}+t_{\mathrm{ir},a}.\end{aligned}\tag{31}$$

According to the definition of $\xi_{i,a}$, the sliding mode variable $S_{i,a}$ is stabilized to the small residual set (17) within a fixed time. Since $S_{i,a}(0)\in\Omega_{si,a}^{\mathrm{r}}$ and $S_{i,a}(0)\notin\Omega_{si,a}$, the negative definite $\dot{V}_{iz,a}$ can be guaranteed. Consequently, $z_{i,a}$ is consistently kept away from infinity. Following the barrier Lyapunov principle, $\xi_{i,a}$ never reaches the preset boundaries, and the sliding mode variable $S_{i,a}$ consistently evolves within the predefined set (17). Therefore, the proof is completed. ■

B. Fixed-time Convergence of Formation Error

In this section, we aim to establish that the formation tracking error achieves the fixed-time convergence and adheres to the prescribed performance constraint upon stabilizing $S_{i,a}$.

Theorem 2: Under the initial condition (16), if the sliding manifold $S_{i,a}$ defined in (15) can be driven into the set (17) within a fixed time, then $\eta_{i,a}$ can be stabilized to the following residual set of (9) within another fixed-time $T_{i\eta,a}$ for $t\geq T_{is,a}+T_{i\eta,a}$

$$\Omega_{i\eta,a}=\left\{\eta_{i,a}\left(t\right)|\underline{\xi}_{is,a}\rho_{i,a}\left(t\right)\leq\eta_{i,a}\left(t\right)\leq\bar{\xi}_{is,a}\rho_{i,a}\left(t\right)\right\},\tag{32}$$

where $T_{i\eta,a}$ is given in (42), representing the settling time bound after $t\geq T_{is,a}$. Furthermore, if the following inequality holds

$$\alpha_{iV,a}=\left(1-k_{iV,a}^{-1}\right)^{p_s/q_s}\min\left\{\bar{\alpha}_{i1,a},\bar{\beta}_{i1,a}\right\}>2k_{i\rho,a},\tag{33}$$

where $\bar{\alpha}_{i1,a}=2^{\frac{m_s+n_s}{2n_s}}\alpha_{i1,a},\bar{\beta}_{i1,a}=2^{\frac{p_s+q_s}{2q_s}}\beta_{i1,a}$ and $k_{iV,a}\in(1,k_{is,a}^{-1})$, then $\eta_{i,a}$ never escapes from the preset boundary in (9), ensuring the achievement of the PPC objective for the desired formation motion.

Proof: i) Firstly, we establish the proof that the system consistently adheres to the predefined performance constraint (8) for any $t\geq0$.

Consider the Lyapunov function $V_{i\eta,a}=\eta_{i,a}^2/2$. Substituting (15) into the time derivative of $V_{i\eta,a}$ produces

$$\dot{V}_{i\eta,a}=-(1-S_{i,a}/\eta_{i,a})^{\frac{p_s}{q_s}}\left(\bar{\alpha}_{i1,a}V_{i\eta,a}^{\frac{m_s+n_s}{2n_s}}+\bar{\beta}_{i1,a}V_{i\eta,a}^{\frac{p_s+q_s}{2q_s}}\right),\tag{34}$$

To elucidate the boundary of $(1-S_{i,a}/\eta_{i,a})$, we introduce the following set

$$\Omega_{i,a}^{\mathrm{mid}}=\left\{\eta_{i,a}(t)|\eta_{i,a}(t)\in\Omega_{i,a},\ \text{and}\ \eta_{i,a}(t)\notin\Omega_{i,a}^{\mathrm{small}}\right\},\tag{35}$$

where $\Omega_{i,a}^{\mathrm{small}}=\{\eta_{i,a}(t)|-k_{iV,a}k_{is,a}k_{i\eta,a}\rho_{i,a}(t)\leq\eta_{i,a}(t)\leq k_{iV,a}k_{is,a}\rho_{i,a}(t)\}$. Then, the condition $\Omega_{i,a}^{\mathrm{small}}\subseteq\Omega_{i,a}$ holds.

Recalling Theorem 1, the PPC constraint (17) for $S_{i,a}$ is ensured by utilizing the designed distributed controller. If the formation tracking error $\eta_{i,a}$ satisfies the inequality of $-k_{i\eta,a}\rho_{i,a}(t)\leq\eta_{i,a}(t)<-k_{iV,a}k_{is,a}k_{i\eta,a}\rho_{i,a}(t)<0$, then the following inequality can be obtained

$$\frac{-S_{i,a}\left(t\right)}{-\eta_{i,a}\left(t\right)}\leq\frac{k_{is,a}k_{i\eta,a}\rho_{i,a}\left(t\right)}{k_{iV,a}k_{is,a}k_{i\eta,a}\rho_{i,a}\left(t\right)}=\frac{1}{k_{iV,a}}<1.\tag{36}$$

If $\eta_{i,a}$ is restricted by $0<k_{iV,a}k_{is,a}\rho_{i,a}(t)\leq\eta_{i,a}(t)<\rho_{i,a}(t)$, we have

$$\frac{S_{i,a}\left(t\right)}{\eta_{i,a}\left(t\right)}\leq\frac{k_{is,a}\rho_{i,a}\left(t\right)}{k_{iV,a}k_{is,a}\rho_{i,a}\left(t\right)}=\frac{1}{k_{iV,a}}<1.\tag{37}$$

From (36) and (37), one can observe that $1-S_{i,a}/\eta_{i,a}>1-k_{iV,a}^{-1}>0$ holds if $\eta_{i,a}\in\Omega_{i,a}^{\mathrm{mid}}$. Then, we have

$$\begin{cases}\dot{V}_{i\eta,a}\leq-\left(1-k_{iV,a}^{-1}\right)^{\frac{p_s}{q_s}}\bar{\alpha}_{i1,a}V_{i\eta,a},\ \ V_{i\eta,a}\geq1,\\ \dot{V}_{i\eta,a}\leq-\left(1-k_{iV,a}^{-1}\right)^{\frac{p_s}{q_s}}\bar{\beta}_{i1,a}V_{i\eta,a},\ \ V_{i\eta,a}<1,\end{cases}\tag{38}$$

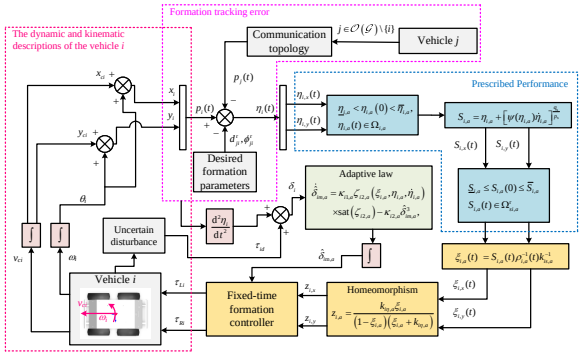

Fig. 3. Formation algorithm flowchart.

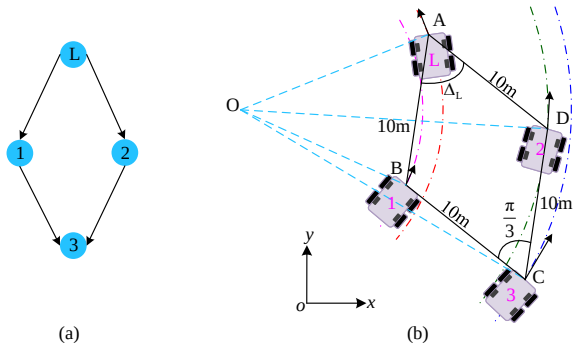

Fig. 4. Information of ideal formation. (a) The communication topology; (b) Reference geometric parameters of rigid formation shapes.

which, when combined with (33), implies that

$$|\eta_{i,a}(t)| = \sqrt{2V_{i\eta,a}} \leq |\eta_{i,a}(0)| e^{-\frac{\alpha_{iV,a}}{2}t} < |\eta_{i,a}(0)| e^{-k_{i\rho,a}t}. \tag{39}$$

Considering the initial condition given in (8), if $\eta_{i,a}(t)$ exponentially decays from $\Omega_{i,a}^{\text{mid}}$ to $\Omega_{i,a}^{\text{small}}$ with $\eta_{i,a}(0) \in \Omega_{i,a}^{\text{mid}}$, it will never violate the preset constraint (9), as indicated by (39). In the case where $\eta_{i,a}(0) \in \Omega_{i,a}^{\text{small}}$, $\eta_{i,a}(t)$ remains within the set $\Omega_{i,a}^{\text{small}}$. Consequently, Theorem 1 consistently ensures that $\eta_{i,a}$ adheres to the PPC constraint (9).

ii) Now, we proceed with the subsequent proof to demonstrate the fixed-time convergence rate of $\eta_{i,a}$.

Let $\Omega_{i\eta,a}^{\text{mid}} = \{\eta_{i,a}(t) | \eta_{i,a}(t) \in \Omega_{i,a}, \text{and } \eta_{i,a}(t) \notin \Omega_{i\eta,a}\}$. Similar to (36) and (37), when $\eta_{i,a}(t) \in \Omega_{i\eta,a}^{\text{mid}}$, we have

$$1 - S_{i,a}(t)\eta_{i,a}^{-1}(t) > 1 - k_{is,a} > 0, \quad t > T_{is,a}, \tag{40}$$

and it follows that

$$\dot{V}_{i\eta,a} \leq (1-k_{is,a})^{p_s/q_s} \left[-\alpha_{i,a} V_{i\eta,a}^{\frac{m_s+n_s}{2n_s}} - \beta_{i,a} V_{i\eta,a}^{\frac{p_s+q_s}{2q_s}} \right]. \tag{41}$$

Invoking Lemma 2, the formation tracking error $\eta_{i,a}$ can be driven to $\Omega_{i\eta,a}$ in a fixed time $T_{i\eta,a}$, as bounded by

$$T_{i\eta,a} = (1-k_{is,a})^{-\frac{p_s}{q_s}} \left[\frac{2n_s}{\bar{\alpha}_{i1,a}(m_s - n_s)} + \frac{2q_s}{\bar{\beta}_{i1,a}(q_s - p_s)} \right]. \tag{42}$$

The proof is now completed. ■

IV. Simulation Examples

In this section, numerical examples are designed based on the algorithm flowchart in Fig. 3 to verify the effectiveness of the proposed leader-steered rigid shape formation framework and the distributed control protocol. The multi-robot vehicles system consists of one leader and three followers, and the corresponding edge set is denoted by $\mathcal{O}(\mathcal{G}) = \{\text{L}, 1, 2, 3\}$. The directed graph $\mathcal{G}$ representing the communication topology is plotted in Fig. 4(a), and the edge set is denoted by $\mathcal{S}(\mathcal{G}) = \{(\text{L}, 1), (\text{L}, 2), (1, 3), (2, 3)\}$. The ideal geometry is given in Fig. 4(b), which is a rhombus with the side length of 10 m, and the interior angle at the leader position is set as $\pi/3$ rad. The vehicle parameters are given as follows: $m = 11.8$ kg, $I_z = 0.153$ kg·m^2, $l = 0.1$ m, $h = 0.15$ m, and $r = 0.075$ m.

The initial conditions are set as follows: $[x_{\text{L}}, y_{\text{L}}, \theta_{\text{L}}]^{\text{T}} = [0, 5, 0]^{\text{T}}$, $[x_1, y_1, \theta_1]^{\text{T}} = [-6, 9, -\pi/12]^{\text{T}}$, $[x_2, y_2, \theta_2]^{\text{T}} = [-3, 2, -\pi/9]^{\text{T}}$, and $[x_3, y_3, \theta_3]^{\text{T}} = [-10, 5, -\pi/3]^{\text{T}}$. The linear velocity of the leader is $v_{c\text{L}} = 1$ m/s, and the angular velocity is given by:

$$\omega_{\text{L}}(t) = \begin{cases} 0, & 0 < t < 20, \\ k_\omega (t-20), & 20 \leq t < 320, \\ 300 k_\omega, & 320 \leq t \leq 470, \end{cases} \tag{43}$$

where $k_\omega = 6.98 \times 10^{-5}$. In addition, $v_{c1}(0)$ =$v_{c2}(0)$=0.3m/s, $v_{c3}(0)$= 0.6 m/s, and $\omega_1(0) = \omega_2(0) = \omega_3(0) = 0$rad/s.

The performance constraint function is formulated as:

$$\rho_{i,a}(t) = (6 - 0.3)\exp(-0.1t) + 0.3, \tag{44}$$

with $k_{i\eta,a} = 0.9$.

The parameters are selected as follows, $m_s = 9, n_s = 5, p_s = 7, q_s = 9, \alpha_{i,a} = 0.2$ and $\beta_{i,a} = 0.3$. The control gains are set as $k_{i\xi,a} = 0.05$ and $k_{is,a} = 0.5$. The parameters in the adaptive law are assigned as $\kappa_{i1,a} = 0.1$ and $\kappa_{i2,a} = 0.05$ for $i = 1, 2, 3$ and $a = x, y$. The value of σ is set to 0.01. The simulation results are depicted in Figs. 5-7.

The trajectories in Fig. 5(a) demonstrate the successful achievement of the proposed leader-steered rigid shape formation defined in Definition 2. Notably, the leading vehicle consistently maintains the foremost position during the formation's movements, steering both translational and rotational motions of the cooperative team. The accuracy of the formation geometry is assessed using two metrics, d_{ji} and Δ_j, as illustrated in Figs. 5(b) and 5(c), respectively. In Fig. 5(b), d_{ji} represents the Euclidean distance between vehicles

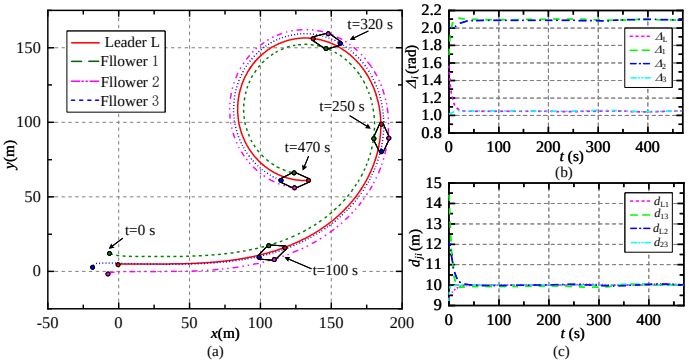

Fig. 5. Simulation results within 470 s. (a) Trajectories; (b) Formation distances d_{ji}; (c) Formation angles Δ_j.

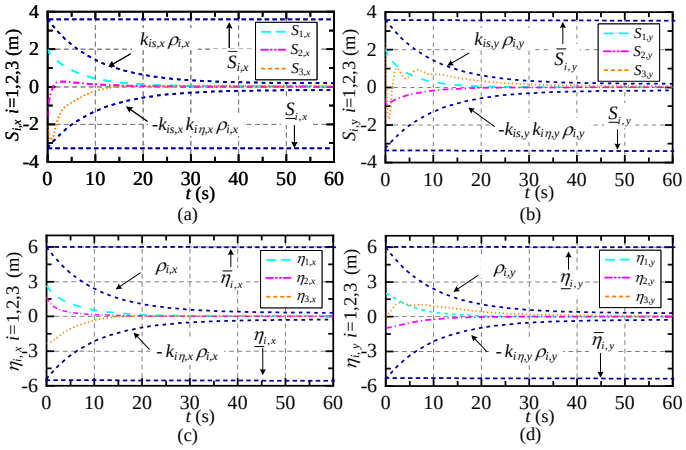

Fig. 6. Convergence of sliding manifolds and formation tracking errors, along with predefined constraints. (a) $S_{i,x}$, (b) $S_{i,y}$, (c) $\eta_{i,x}$, (d) $\eta_{i,y}$.

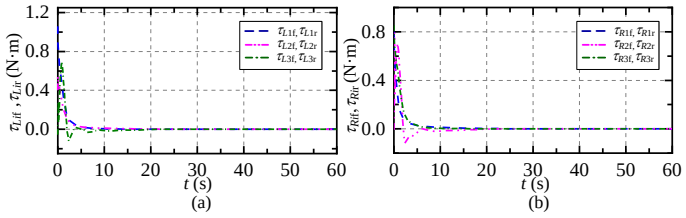

Fig. 7. Control inputs of a single wheel of vehicle i. (a) τ_{Lif} and τ_{Lir}, (b) τ_{Rif} and τ_{Rir} ($\tau_{L(R)if} = \tau_{L(R)ir} = \tau_{L(R)i}/2, i = 1, 2, 3$).

j and i, while the graphical description of Δ_j is presented in Fig. 5(c), representing the interior angle at vertex p_j in the formation. These results indicate that the proposed formation protocols ensure the desired geometric distances and angles for the rigid shape formation of the multi-robot vehicles. Moreover, it is noteworthy that the cooperative team achieves both translational and rotational movements without relying on the consensus direction condition, as depicted in Fig. 5.

In Figs. 6(a) and 6(b), it is evident that the proposed nonsingular sliding manifolds for the three following vehicles consistently evolve within the predefined constraints, affirming the effectiveness of the control protocol outlined in Theorem 1. Adhering to the necessary condition specified in Theorem 2 for the controller parameters, the formation tracking errors of the following vehicles along the x-axis and y-axis are stabilized to the neighborhood of zero. Moreover, the prescribed performance constraints are rigorously maintained, as illustrated in Figs. 6(c) and 6(d). The distributed control inputs for the following vehicles are depicted in Fig. 7.

V. Experiment Studies

To validate the practical applicability of the proposed formation control protocol, experiments are conducted using four robotic vehicles, as depicted in Fig. 8. The control protocol is implemented using a Jetson Nano B01 (with a 128-Core Maxwell GPU, 4-Core ARM A57, 4GB 64Bit LPDDR4, Linux) to facilitate communication with neighboring vehicles via a 5G wireless network. At the vehicle's bottom layer controller, a core board with STM32 (F103RCT6) is

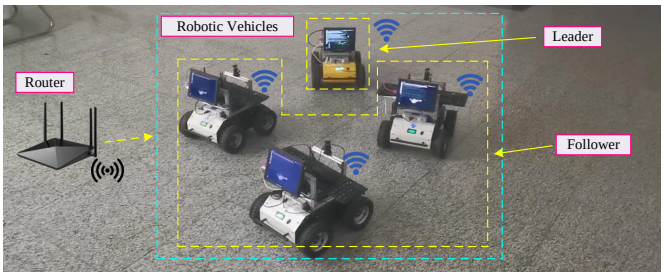

Fig. 8. Experimental setup

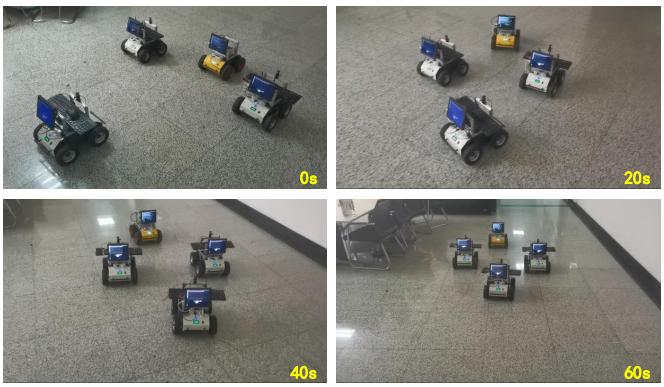

Fig. 9. Formation process from a recorded video during the experiment.

employed to execute the calculated inputs on the vehicle motors. The odometer, integrating the inertial measurement unit (MPU6050) and the motor encoder, provided accurate vehicle position and motion information. Notably, each robotic vehicle is configured with identical settings.

A. Experimental Validation

The implementation of the directed graph for the communication topology is the same as in the simulations. Additionally, due to space limitations in the experiments, the edge length of the target formation geometry is set to 0.9 m, while other formation and vehicle parameters remain consistent with those used in the simulations in Section IV.

The initial conditions are specified as follows: $[x_{\mathrm{L}}, y_{\mathrm{L}}, \theta_{\mathrm{L}}]^{\mathrm{T}} = [0.52, -0.3, 0]^{\mathrm{T}}$, $[x_1, y_1, \theta_1]^{\mathrm{T}} = [0.14, 0.45, 0]^{\mathrm{T}}$, $[x_2, y_2, \theta_2]^{\mathrm{T}} = [0.14, -0.95, 0]^{\mathrm{T}}$, and $[x_3, y_3, \theta_3]^{\mathrm{T}} = [-1.12, -0.1, 0]^{\mathrm{T}}$. The linear velocity of the leader is set to $v_{c\mathrm{L}} = 0.1$ m/s, and the angular velocity is given by:

$$\omega_{\mathrm{L}}(t) = \begin{cases} 0 & t < 5, \\ 0.00129\pi(\mathrm{t} - 5) & 5 \le t < 25, \\ 0.00129\pi(45 - \mathrm{t}) & 25 \le t < 45, \\ 0 & 45 \le t \le 70. \end{cases} \tag{45}$$

In addition, $v_{c1}(0)$ =$v_{c2}(0)$=$v_{c3}(0) = 0.1$ m/s and $\omega_1(0) = \omega_2(0) = \omega_3(0) = 0$ rad/s.

The performance constraint function is defined as:

$$\rho_{i,a}(t) = (0.7 - 0.07)\exp(-0.06t) + 0.07, \tag{46}$$

with $k_{i\eta,a} = 1.2$.

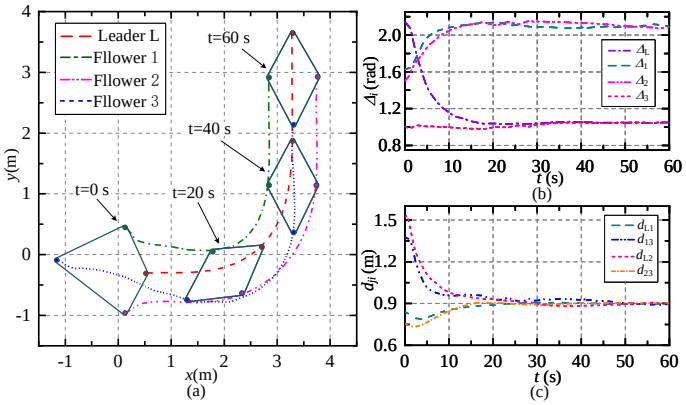

Fig. 10. Experiment results within 60 s. (a) Trajectories; (b) Formation distances d_{ji}; (c) Formation angles Δ_j.

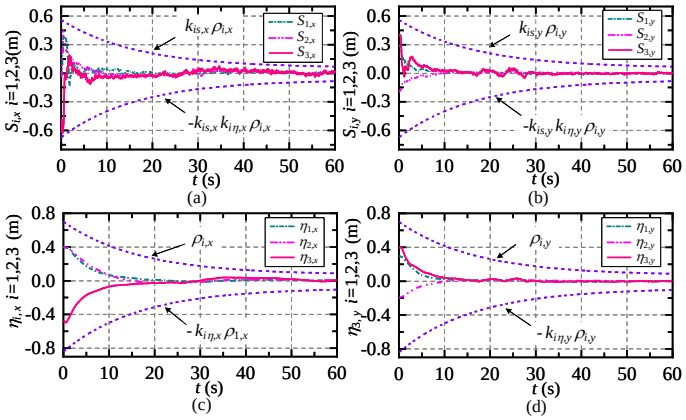

Fig. 11. Convergence of sliding manifolds and formation tracking errors, along with predefined constraints. (a) $S_{i,x}$, (b) $S_{i,y}$, (c) $\eta_{i,y}$, (d) $\eta_{i,y}$.

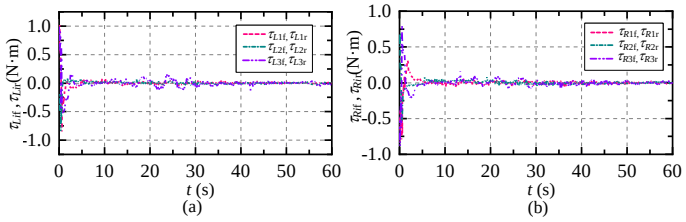

Fig. 12. Control inputs of a single wheel of vehicle i. (a) τ_{Lif} and τ_{Lir}, (b) τ_{Rif} and τ_{Rir} ($\tau_{L(R)if} = \tau_{L(R)ir} = \tau_{L(R)i}/2, i = 1, 2, 3$).

Select $m_s = 9, n_s = 5, p_s = 7, q_s = 9, \alpha_{i,a} = 0.1$, and $\beta_{i,a} = 0.15$. The control gains are set as $k_{i\xi,a} = 0.2$ and $k_{is,a} = 0.8$. The parameters in the adaptive law are set by $\kappa_{i1,a} = 0.1$ and $\kappa_{i2,a} = 0.05$ for $i = 1, 2, 3$ and $a = x, y$. The value of σ is set to 0.01. The experiment results are plotted in Figs. 9-12.

In Fig. 9, we present snapshots of the experimental formation process at $t = 0$ s, 20 s, 40 s, and 60 s. The trajectories of the multi-vehicle formation system are illustrated in Fig. 10(a), while the evolution of the formation geometry is shown in Figs. 10(b) and 10(c). Based on these experimental results, it is evident that the controlled following vehicles perform the ideal formation motions with the leading vehicle, forming the

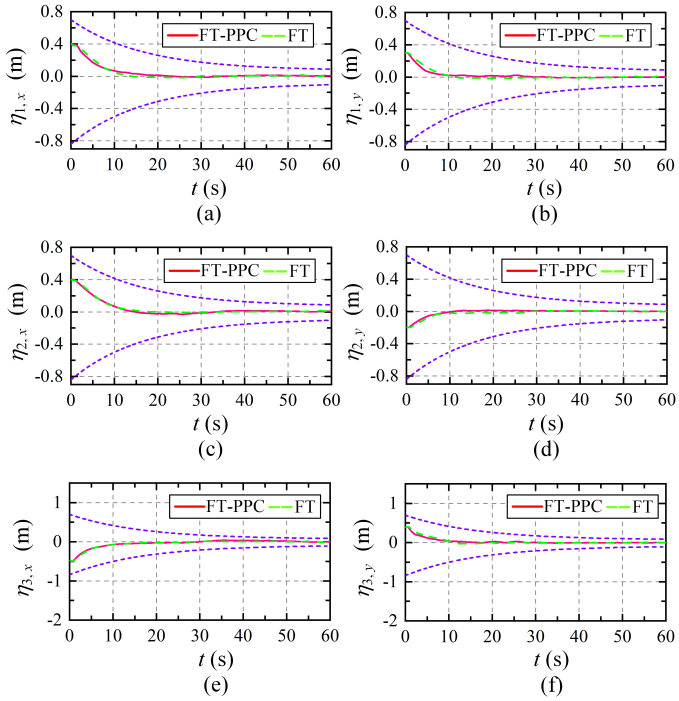

Fig. 13. Experiment comparison results of formation tracking errors. (a)-(b) Formation tracking errors for vehicle 1, (c)-(d) Formation tracking errors for vehicle 2, (e)-(f) Formation tracking errors for vehicle 3.

desired geometry outlined in Definition 2. Additionally, the experimental results in Fig. 11 indicate that the sliding manifolds and formation tracking errors consistently adhere to the prescribed performance constraints, ultimately converging to a small neighborhood of zero. Fig. 12 provides insights into the actual torques applied to the wheels of the following vehicles during the formation experiment. Hence, these experimental results affirm the effectiveness of the leader-steered rigid shape formation model and the fixed-time control algorithm for the prescribed performance as proposed in this paper.

B. Comparison analysis

To evaluate the control performance, we conduct a comparative analysis between our proposed control protocol (abbreviated as "FT-PPC" in the figures) and a conventional fixed-time control method without prescribed performance [12] (abbreviated as "FT" in the figures). The construction of the conventional fixed-time controller is as follows:

$$u_{i,a} = -\psi_{i,a}^{-1}\left(c_{i1,a} + c_{i2,a} + c_{i3,a}\right), \tag{47}$$

with

$$\begin{cases} c_{i1,a} = \psi_{i,a}\left(g_{i,a} + \hat{\delta}_{im,a}\,\mathrm{sat}\left(\zeta_{i1,a}\right)\right), \\ c_{i2,a} = -\alpha_{i,a}\left(m_s/n_s - p_s/q_s\right)\eta_{i,a}^{m/n-p/q-1}\left(\psi_{i,a}\dot{\eta}_{i,a}\right)^2, \\ c_{i3,a} = \left[\dfrac{q_s}{p_s}\left(\psi_{i,a}\dot{\eta}_{i,a}\right)^{q_s/p_s-1}\right]^{-1}\dot{\eta}_{i,a} \\ \qquad + \dfrac{q_s}{p_s}\left(\psi_{i,a}\right)^{-q_s/p_s}\mu\left(\dot{\eta}_{i,a}^{q_s/p_s-1}\right) \\ \qquad \dot{\eta}_{i,a}^{1-q_s/p_s}\left(\alpha_{if,a}S^{m_f/n_f} + \beta_{if,a}S^{p_f/q_f}\right), \end{cases}$$

where the controller parameters are selected as $m_s = 9, n_s = 5, p_s = 7, q_s = 9, \alpha_{i,a} = 0.07$, and $\beta_{i,a} = 0.2$.

The comparative results are depicted in Fig. 13. After numerous attempts to fine-tune the parameters of the conventional fixed-time controller, it becomes apparent that this approach closely approximates the performance achieved by our proposed control method while maintaining the formation errors within the predefined boundaries. However, it is crucial to note that, with the conventional fixed-time control method, we cannot predict whether the formation errors will remain within the predefined boundaries until we complete these tuning attempts and obtain the results. This underscores the advantage of our proposed control protocol, which has the capability to predict and achieve specific control performance criteria.

VI. Conclusion

This article introduces a novel formation framework and a distributed fixed-time formation control protocol with the prescribed performance. In contrast to conventional consensus-based formation control, our proposed leader-steered rigid shape formation aims to establish and maintain a consistent invariant formation geometry. The entire formation shape dynamically follows the leader's motion, accommodating both translational and rotational movements. By incorporating a nonsingular fixed-time sliding manifold, our distributed formation control protocol ensures the stabilization of formation tracking errors within a fixed time, while also guaranteeing adherence to preset constraints. Finally, the protocol successfully achieves the proposed leader-steered rigid shape formation. This comprehensive approach contributes to advancing the field of multi-robot systems, offering enhanced control precision and adaptability in real-world scenarios.

Appendix
Analysis of the transgress process of $\dot{\eta}_{i,a}$

Invoking Lemma 2, if $z_{i,a}$ exits the region defined in $V_{iz\mathrm{m},a}$ as given in (29), (27) can be further expressed as the following inequality with either $0 < |\dot{\eta}_{i,a}| \leq \sigma^{p_s/q_s - p_s}$ or $|\dot{\eta}_{i,a}| > \sigma^{p_s/q_s - p_s}$,

$$\begin{aligned}\dot{V}_{iz,a} \leq & -\underbrace{\left(1 - \varpi_{i1,a} - \varpi_{i2,a} - \varpi_{i3,a}\right)\chi_{i1,a}}_{\varpi_{i4,a}>0} V_{iz,a}^2 \\ & - \chi_{i2,a} V_{iz,a}^{\lambda_{i,a}} \\ \leq & -\varpi_{i4,a} V_{iz,a},\end{aligned} \tag{48}$$

which implies that $z_{i,a} \leq \sqrt{2V_{iz,a}} \leq z_{i,a}(0)\sqrt{2}e^{-(\varpi_{i4,a}/2)t}$, and $z_{i,a}$ is bounded by a monotonically decreasing boundary.

Indeed, $z_{i,a}$, which initially exhibits fixed-time convergence, is intentionally modified to undergo a degeneration towards asymptotic convergence. This modification serves to specifically illustrate that $\dot{\eta}_{i,a}$ will not repeatedly enter the region $|\dot{\eta}_{i,a}| \leq \sigma^{p_s/q_s - p_s}$.

According to the homeomorphic mapping of $S_{i,a}$, $\xi_{i,a}$ and $z_{i,a}$, we can deduce that $S_{i,a}$ is also constrained by a monotonically decreasing boundary. Referring to the definition of $S_{i,a}$ in (15) with $0 < |\dot{\eta}_{i,a}| \leq \sigma^{p_s/q_s - p_s}$, we have

$$\begin{aligned}\dot{\eta}_{i,a} = & \left(S_{i,a}\eta_{i,a}^{-1} - 1\right)^{p_s/q_s} \Big(\alpha_{i,a}|\eta_{i,a}|^{m_s/n_s} \\ & + \beta_{i,a}|\eta_{i,a}|^{p_s/q_s}\Big) \operatorname{sign}\left(\eta_{i,a}\right).\end{aligned} \tag{49}$$

Now, we are ready to demonstrate that if $\dot{\eta}_{i,a}$ is initially in the region $|\dot{\eta}_{i,a}| \leq \sigma^{p_s/q_s - p_s}$, it will exit this region and will not return unless $\eta_{i,a}$ has converged to a neighborhood of zero.

Since the sliding manifold $S_{i,a}$ is an attractor, as demonstrated in Theorem 1, both $\dot{\eta}_{i,a}$ and $\eta_{i,a}$ are attracted into the region defined in (21). According to the sliding mode scheme, $S_{i,a}$ converges before $\dot{\eta}_{i,a}$ and $\eta_{i,a}$ converge to the neighborhood of zero. Considering a large $\eta_{i,a} > 0$ that has not yet converged and a sufficient small σ, the converging $S_{i,a}$, bounded by a monotonically decreasing boundary according to (48), will drive $\left(S_{i,a}\eta_{i,a}^{-1} - 1\right)$ to -1. This will result in a monotonically decreasing negative $\dot{\eta}_{i,a}$, causing $\dot{\eta}_{i,a}$ to exit the small region $|\dot{\eta}_{i,a}| \leq \sigma^{p_s/q_s - p_s}$ with a large value of $\left(\alpha_{i,a}|\eta_{i,a}|^{m_s/n_s} + \beta_{i,a}|\eta_{i,a}|^{p_s/q_s}\right)$ before $\eta_{i,a}$ has converged to the neighborhood of zero. Therefore, once $\dot{\eta}_{i,a}$ exits the region $|\dot{\eta}_{i,a}| \leq \sigma^{p_s/q_s - p_s}$, it will not return to this region until $\eta_{i,a}$ has converged.

A similar result can also be obtained when $\eta_{i,a} < 0$. After $\eta_{i,a}$ and $\dot{\eta}_{i,a}$ have been attracted into the neighborhood region of the sliding manifold $S_{i,a}$, $\dot{\eta}_{i,a}$ will re-enter and consistently remain within the region $|\dot{\eta}_{i,a}| < \sigma^{p_s/(q_s - p_s)}$. This re-entry occurs because the control objective has been achieved with the converged $\eta_{i,a}$ and sufficient small $\dot{\eta}_{i,a}$, simultaneously.

References

[1] S. J. Yoo and B. S. Park, "Distributed adaptive formation tracking for a class of uncertain nonlinear multiagent systems: guaranteed connectivity under moving obstacles," *IEEE Trans. Cybern., early access*, Apr. 2023.

[2] S. He, M. Wang, S. Dai and F. Luo, "Leader-follower formation control of USVs with prescribed performance and collision avoidance," *IEEE Trans. Industr. Inform.*, vol. 15, no. 1, pp. 572-581, Jan. 2019.

[3] D. Li and G. Guo, "Prescribed performance concurrent control of connected vehicles with nonlinear third-Order dynamics," *IEEE Trans. Veh. Technol.*, vol. 69, no. 12, pp. 14793-14802, Dec. 2020.

[4] W. Liu, X. Wang and S. Li, "Formation control for leader follower wheeled mobile robots based on embedded control technique," *IEEE Trans. Control Syst. Technol.*, vol. 31, no. 1, pp. 265-280, Jan. 2023.

[5] L. Consolini, F.Morbidi, D. Prattichizzo and M. Tosques, "Leader-follower formation control of nonholonomic mobile robots with input constraints," *Automatica*, vol. 44, no. 5, pp. 1343-1349, May. 2008.

[6] Y. Mei, Y. H. Lu, Y. C. Hu, and C. G. Lee, "Deployment of mobile robots with energy and timing constraints," *IEEE Trans. Robot.*, vol. 22, no. 3, pp. 507-522, Jun. 2006.

[7] S. Sui, C. L. P. Chen and S. Tong, "A novel full errors fixed-time control for constraint nonlinear systems," *IEEE Trans. Automat. Contr.*, vol. 68, no. 4, pp. 2568-2575, Apr. 2023.

[8] Z. Zuo, L. Tie, "Distributed robust finite-time nonlinear consensus protocols for multi-agent systems," *Int. J. Syst. Sci.*, vol. 47, no. 6, pp.1366-1375, Jun. 2014.

[9] S. Chang, Y. Wang, Z. Zuo and H. Yang, "Fixed-time formation control for wheeled mobile robots with prescribed performance," *IEEE Trans. Control. Syst. Technol.*, vol. 30, no. 2, pp. 844-851, Mar. 2022.

[10] C. Wang, H. Tnunay, Z. Zuo, B. Lennox and Z. Ding, "Fixed-time formation control of multirobot systems: design and experiments," *IEEE Trans. Ind. Electron.*, vol. 66, no. 8, pp. 6292-6301, Aug. 2019.

[11] D. Wu, H. Du, G. Wen and J. L, "Fixed-time synchronization control for a class of master slave systems based on homogeneous method," *IEEE Trans. Circuits Syst. II*, vol. 66, no. 9, pp. 1547-1551, Sept. 2019.

[12] Z. Zuo. "Nonsingular fixed-time consensus tracking for second-order multi-agent networks," *Automatica*, vol. 54, pp. 305-309, Apr. 2015.
[13] N. Wang, S. Lv, M. J. Er and W. -H. Chen, "Fast and accurate trajectory tracking control of an autonomous surface vehicle with unmodeled dynamics and disturbances," *IEEE Trans. Intell. Veh.*, vol. 1, no. 3, pp. 230-243, Sept. 2016.
[14] X. Bu, M. Lv, H. Lei and J. Cao, "Fuzzy neural pseudo control with prescribed performance for waverider vehicles: a fragility-avoidance approach," *IEEE Trans. Cybern.*, vol. 53, no. 8, pp. 4986-4999, Aug. 2023.
[15] Z. Liang, Z. Wang, J. Zhao and P . K. Wong, "Fixed-time prescribed performance path-following control for autonomous vehicle with complete unknown parameters," *IEEE Trans. Ind. Electron.*, vol. 70, no. 8, pp. 8426-8436, Aug. 2023.
[16] J. Gong, B. Jiang, Y. Ma and Z. Mao, "Distributed adaptive fault-tolerant formation-containment control with prescribed performance for heterogeneous multiagent systems," *IEEE Trans. Cybern.*, vol. 53, no. 12, pp. 7787-7799, Dec. 2023.
[17] B. Tian, H. Lu, Z. Zuo and W. Yang, "Fixed-time leader-follower output feedback consensus for second-order multiagent systems," *IEEE Trans. Cybern.*, vol. 49, no. 4, pp. 1545-1550, Apr. 2019.
[18] M. Hua, H. Ding, X.-Y. Yao and X. Zhang, "Distributed fixed-time formation-containment control for multiple Euler-Lagrange systems with directed graphs," *Int. J. Control. Autom. Syst.*, vol. 19, no. 2, pp. 837-849. Feb. 2021.
[19] S. Shi, S. Xu, W. Liu and B. Zhang, "Global Fixed-time consensus tracking of nonlinear uncertain multiagent systems with high-order dynamics," *IEEE Trans. Cybern.*, vol. 50, no. 4, pp. 1530-1540, Apr. 2020.
[20] X. You, C. Hua, K. Li and X. Jia, "Fixed-time leader-following consensus for high-order time-varying nonlinear multiagent dystems," *IEEE Trans. Automat. Contr.*, vol. 65, no. 12, pp. 5510-5516, Dec. 2020.
[21] J. Ni and P. Shi, "Adaptive neural network fixed-time leader-follower consensus for multiagent systems with constraints and disturbances," *IEEE Trans. Cybern.*, vol. 51, no. 4, pp. 1835-1848, April 2021.
[22] X. Yu and L. Liu, "Distributed formation control of nonholonomic vehicles subject to velocity constraints," *IEEE Trans. Ind. Electron.*, vol. 63, no. 2, pp. 1289-1298, Feb. 2016.
[23] Y. Liu, X. Dong, P. Shi, Z. Ren and J. Liu, "Distributed fault-tolerant formation tracking control for multiagent systems with multiple leaders and constrained actuators," *IEEE Trans. Cybern.*, vol. 53, no. 6, pp. 3738-3747, Jun. 2023.
[24] W. Wang, J. Huang, C. Wen, and H. Fan, "Distributed adaptive control for consensus tracking with application to formation control of nonholonomic mobile robots," *Automatica*, vol. 50, no. 4, pp. 1254-1263, Apr. 2014.
[25] H. Du, W. Zhu, G. Wen, Z. Duan and J. L, "Distributed formation control of multiple quadrotor aircraft based on nonsmooth consensus algorithms," *IEEE Trans. Cybern.*, vol. 49, no. 1, pp. 342-353, Jan. 2019.
[26] H. G. de Marina, "Maneuvering and robustness issues in undirected displacement-consensus-based formation control," *IEEE Trans. Automat. Contr.*, vol. 66, no. 7, pp. 3370-3377, Jul. 2021.
[27] W. Wang, Z. Han, K. Liu and J. L, "Distributed adaptive resilient formation control of uncertain nonholonomic mobile robots under deception attacks," *IEEE Trans. Circuits. Syst. I Regul. Pap.*, vol. 68, no. 9, pp. 3822-3835, Sept. 2021.
[28] Z. Huang, R. Bauer and Y. -J. Pan, "Event-triggered formation tracking control with application to multiple mobile robots," *IEEE Trans. Ind. Electron.*, vol. 70, no. 1, pp. 846-854, Jan. 2023.
[29] Z. Wang, L. Wang, H. Zhang, L. Vlacic and Q. Chen, "Distributed formation control of nonholonomic wheeled mobile robots subject to longitudinal slippage constraints," *IEEE Trans. Syst. Man Cybern. Syst.*, vol. 51, no. 5, pp. 2992-3003, May 2021.
[30] F. Xiao, L. Wang, J. Chen, and Y. Gao, "Finite-time formation control for multi-agent systems," *Automatica*, vol. 45, no. 11, pp. 2605-2611, Nov. 2009.
[31] L. Ma, F. Zhu, J. Zhang and X. Zhao. "Leader-follower asymptotic consensus control of multiagent systems: an observer-based disturbance reconstruction approach," *IEEE Trans. Cybern.*, vol. 53, no. 2, pp. 1311-1323, Feb. 2023.
[32] Y. -W. Chen, M. -L. Chiang and L. -C. Fu, "Three-dimensional maneuver control of multiagent systems with constrained input," *IEEE Trans. Cybern.*, vol. 53, no. 10, pp. 6133-6145, Oct. 2023.
[33] Z. Miao, H. Zhong, Y. Wang, H. Zhang, H. Tan and R. Fierro, "Low-complexity leader-following formation control of mobile robots using only FOV-constrained visual feedback," *IEEE Trans. Industr. Inform.*, vol. 18, no. 7, pp. 4665-4673, July 2022.
[34] X. Liang, Y. -H. Liu, H. Wang, W. Chen, K. Xing and T. Liu, "Leader-following formation tracking control of mobile robots without direct position measurements," *IEEE Trans. Automat. Contr.*, vol. 61, no. 12, pp. 4131-4137, Dec. 2016.
[35] Y. Ai and H. Wang, "Fixed-time anti-synchronization of unified chaotic systems via adaptive backstepping approach," *IEEE Trans. Circuits Syst. II: Express Br.*, vol. 70, no. 2, pp. 626-630, Feb. 2023.
[36] P. Yang and Y. Su, "Proximate fixed-time prescribed performance tracking control of uncertain robot manipulators," *IEEE/ASME Trans. Mechatron.*, vol. 27, no. 5, pp. 3275-3285, Oct. 2022.
[37] M. L. Nguyen, X. Chen and F. Yang, "Discrete-time quasi-sliding-mode control with prescribed performance function and its application to piezo-actuated positioning systems," *IEEE Trans. Ind. Electron.*, vol. 65, no. 1, pp. 942-950, Jan. 2018.
[38] J. Guo, Q. Peng and Z. Guo, "SMC-based integrated guidance and control for beam riding missiles with limited LBPU," *IEEE Trans. Aerosp. Electron. Syst.*, vol. 57, no. 5, pp. 2969-2978, Oct. 2021.
[39] Z. Liang, J. Zhao, Z. Dong, Y. Wang and Z. Ding, "Torque vectoring and rear-wheel-steering control for vehicle's uncertain slips on soft and slope terrain using sliding mode algorithm," *IEEE Trans. Veh. Technol.*, vol. 69, no. 4, pp. 3805-3815, Apr. 2020.
[40] X. He, J. Zhai and Z. Geng, "Roto-translation invariant formation of multiple underactuated planar rigid bodies," *IEEE Trans. Cybern.*, vol. 52, no. 12, pp. 12818-12831, Dec. 2022.
[41] S. Dai, K.Lu , X. Jin, "Fixed-time formation control of unicycle-type mobile robots with visibility and performance constraints," *IEEE Trans. Ind. Electron.*, vol. 68, no. 12, pp. 12615-12625, Dec. 2021.

Zhongchao Liang (Member, IEEE) received his M.S. and Ph.D. degrees in Mechanical Engineering from Harbin Institute of Technology, China, in 2011 and 2015, respectively. From 2019 to 2020, he was an academic visitor with the Department of Electrical and Electronic Engineering, the University of Manchester, UK.

He is currently an Associate Professor with School of Mechanical Engineering and Automation, Northeastern University, China. His research interests include nonlinear and adaptive control for intelligent vehicles and mobile robots, and distributed control for multi-agent systems.

Chunxiao Lyu received the B.S. degrees in Mechanical Engineering from Ningxia University, Ningxia, China, in 2020, respectively.

He is currently pursing the Master's degree in School of Mechanical Engineering and Automation, Northeastern University, Shenyang, China. His research is on the topic of prescribed performance control and formation control of multiple vehicles.

Mingyu Shen (Student Member, IEEE) received the B.S. degree in Vehicle Engineering from Beihua University, Jilin, China, in 2019, the M.S. degree in Transportation Engineering from Northeast Forestry University, Harbin, China, in 2022. He is currently working toward the Ph.D. degree in School of Mechanical Engineering and Automation, Northeastern University, Shenyang, China.

His research interests include nonlinear control and cooperative control on multi-agent systems.

Jing Zhao received the Ph.D. degree in electromechanical engineering from University of Macau, Macao, China, in 2016. He is currently working with School of Mechanical Engineering and Automation, Northeastern University, China. His research interests include dynamics and control, mechanism and machine theory, fluid mechanics, and finite element analysis.

Zhongguo Li (Member, IEEE) received the B.Eng. and Ph.D. degrees in electrical and electronic engineering from the University of Manchester, Manchester, U.K., in 2017 and 2021, respectively.

He is currently a Lecturer (Assistant Professor) in Robotics, Control, Communication and AI at the University of Manchester. Before joining Manchester, he was a Lecturer at University College London and a Research Associate at Loughborough University. His research interests include optimization and decision-making for advanced control, distributed algorithm development for game and learning in network connected multi-agent systems, and their applications in robotics and autonomous vehicles.

Zhengtao Ding (SM'03) received B.Eng. degree from Tsinghua University, Beijing, China, and M.Sc. degree in systems and control, and the Ph.D. degree in control systems from the University of Manchester Institute of Science and Technology, Manchester, U.K. After working as a Lecturer with Ngee Ann Polytechnic, Singapore, for ten years, he joined the University of Manchester in 2003, where he is currently Professor of Control Systems with the Dept. of Electrical and Electronic Engineering.

His research interests include nonlinear and adaptive control theory and their applications, more recently network-based control, distributed optimization and distributed machine learning, with applications to power systems and robotics.